Stability and nonlinear dynamics of a settling fresh water particle laden fluid below a salt water layer

C. Reyes, C. F. Ihle

Department of Mining Engineering, and
Advanced Mining Technology Center, Universidad de Chile
cristian.reyes@ug.uchile.cl

C. Arratia

Departamento de Física, FCFM, Universidad de Chile, and
Nordita, KTH Royal Institute of Technology and Stockholm University
Roslagstullsbacken 23, SE-106 91 Stockholm, Sweden

Abstract

We present a numerical study of the evolution of a semi-infinite layer of salt water over a sedimenting fresh-water suspension. Depending on a proposed ratio between the excess densities of the two layers, we observe the development of Rayleigh-Taylor like instabilities or upwelling fresh water plumes. When Rayleigh-Taylor like instabilities occurr, sediment particles are suspended onto the top layer as well as deep penetration of salt into the bottom layer. When fresh water plumes are observed, a controlled mixing process occurs in which fresh water rises as the particles sediment and there is limited penetration of salt on the bottom layer. Dimensional analysis and an analogy with the mechanism of thermal plume ejection in Rayleigh-Bénard convection are used to propose relevant time and length scales.

1 Introduction

Hyperpycnal flows are defined as subaqueous sediment-transporting density flows where the solid-liquid ensemble is heavier than the ambient where the discharge takes place. They have been first reported in the late 19th century, and are commonly found in lakes and the ocean (Mulder et al., 2003).

A special class, and comparatively less studied related flow, are lofting gravity flows (also referred to herein as *lofting flows*). They are particle-laden gravity currents, where a density inversion by interstitial fluid lower in density than the ambient occurs, enabling the possibility of a flow separation *via* plume detachment. The conditions and evolution of the plume detachment mechanism is not fully understood. In particular, in an otherwise quiescent two-horizontal-layer system, the separation mechanism occurring when the bulk of the suspension is denser than the upper layer but the fluid in the upper layer is heavier that the fluid in the bottom suspension is not quiescent, and may feature a Rayleigh-Taylor instability or mixing in the upper layer *via* plume formation. This particular configuration has been recently studied by Schulte et al. (2016) when both particles and salt are dissolved in the bottom and top layers, respectively. In the present paper, this restriction is relaxed and a mixture model, suitable for higher concentrations and to account for the effect of particle drag by the fluid flow, has been adapted. The onset of mixing in two identified flow regimes is discussed in light of a characteristic time scale.

2 Governing Equations

We consider a semi-infinite layer of salt water on top of a semi-infinite layer of a fresh water suspension. The suspension is modeled as a continuum with solid velocity, density and volume fraction fields $\mathbf{u}_s, \rho_s$ and $\phi_s \equiv \phi$, respectively, superimposed to the liquid with velocity $\mathbf{u}_l$, density ρ_l and volume fraction $\phi_l = 1 - \phi$. The momentum conservation equations are:

$$\frac{\partial(\phi_i \rho_i \mathbf{u}_i)}{\partial t} + \nabla \cdot (\phi_i \rho_i \mathbf{u}_i \mathbf{u}_i) + \nabla \cdot (\phi_i \boldsymbol{\tau}_i) = -\phi_i \nabla p + \phi_i \rho_i \mathbf{g} + \mathbf{f}_i, \tag{1}$$

where the subindex i stands for solid (s) or liquid (l). The presure p, assumed common to both phases, imposes the conservation of volume by enforcing incompressibility of the mean velocity

$$\nabla \cdot (\phi_l \mathbf{u}_l + \phi_s \mathbf{u}_s) = 0. \tag{2}$$

An additional solid pressure contribution $p_s(\phi)$, which sharply increases around the maximum packing fraction ϕ_{max}, is added on the momentum equation for the solid in order to bound the volume fraction of solid ϕ below $\phi_{max} = 0.65$. This extra pressure term is negligible for the small and moderate ϕ present around the interface. The shear stress tensor for each phase is given by

$$\boldsymbol{\tau}_i = \mu_i \left(\frac{\nabla \mathbf{u}_i + (\nabla \mathbf{u}_i)^T}{2} - \frac{2}{3} (\nabla \cdot \mathbf{u}_i) \mathbf{I} \right) \tag{3}$$

where the effective viscosity of the solid μ_s is obtained from

$$\mu_{mix} = \phi \mu_s + (1 - \phi) \mu_l = \mu_l \left(1 - \frac{\phi}{\phi_{max}} \right)^{-\eta[\phi_{max}]} \tag{4}$$

which is the expression for the viscosity of suspensions given by Enwald et al. (1996).

The remaining interaction between the liquid and solid phases is given by the drag force per unit volume $\mathbf{f}_D = \mathbf{f}_s = -\mathbf{f}_l$ that the fluid applies on the solid, which is given by

$$\mathbf{f}_D = K(\mathbf{u}_l - \mathbf{u}_s), \tag{5}$$

where we use the drag function K given by Gidaspow (1986),

$$K = \frac{3}{4d} C_D \phi \rho_l |\mathbf{u}_l - \mathbf{u}_s| (1 - \phi)^{-1.65}, \tag{6}$$

with d the diameter of the sediment's particles and the drag coefficient C_D given by Schiller and Naumann (1935) as

$$C_D = 24(1 + 0.15(Re_p)^{0.687})/Re_p, \tag{7}$$

where $Re_p = \rho_l |\mathbf{u}_l - \mathbf{u}_s| d / \mu_l$ is the particle's Reynolds number.

The density of the liquid is assumed to depend linearly on the salt concentration S as

$$\rho_l = \rho_{l0}(1 + \alpha S) \tag{8}$$

where ρ_{l0} is the density of fresh water and α is an expansion coefficient. The salt concentration satisfies the advection diffusion equation

$$\frac{\partial S}{\partial t} + \nabla \cdot (S \mathbf{u}) = D \nabla^2 S, \tag{9}$$

where D is the diffusion coefficient of salt in water. Finally, the mass transport equation for the solid phase is

$$\frac{\partial(\phi\rho_s)}{\partial t} + \nabla\cdot(\phi\rho_s\mathbf{u}) = \kappa\nabla^2\phi\rho_s, \tag{10}$$

wherein the diffusivity κ accounts for brownian motion and is taken equal to $D/25$.

In the initial condition, the salt concentration of the top layer is S_0 such that $\alpha S_0 = 0.0245$, and the volume fraction of particles in the bottom layer is ϕ_0.

3 Dimensional analysis

From the system of equations defined above, we consider as independent variables the particle settling velocity within the Stokes regime (w_s at small particle Reynolds number), ν, D, the initial density excess due to salt in the upper layer (αS_0), the solid phase and clear water phase densities, ρ_s and ρ_{l0}, respectively, and the initial particle volume fraction in the lower layer, ϕ_0. Noting that the problem also depends explicitly on the magnitude of gravity, g, by virtue of the Buckingham theorem, there must be 5 independent dimensionless numbers. Both ϕ_0 and αS_0 are dimensionless. On the other hand, the relative thickness of between the momentum and the salt diffusion boundary layers in the liquid phase is expressed as the Schmidt number, $Sc = \nu/D$.

It is hypothesized that a relevant dimensionless number is the ratio between the excess density of the upper layer (8) (initially clear, salt water) and the excess bulk density of the lower layer (initially particle laden fresh water), which yields the dimensionless number $\frac{\rho_l(S=S_0)-\rho_{l0}}{\rho_m(\phi=\phi_0,S=0)-\rho_{l0}}$, with $\rho_m = \phi_0\rho_s + (1-\phi_0)\rho_l$:

$$R_\rho = \frac{\alpha S_0}{\phi_0(G-1)}, \tag{11}$$

where $G = \rho_s/\rho_{l0}$. From the relative difference between the slurry and the clear water density, the dimensionless number Λ is written as $\Lambda = (\rho_m - \rho_{l0})/\rho_{l0} = \alpha S_0(1-\phi_0) + (G-1)\phi_0$. In terms of R_ρ,

$$\Lambda = \frac{\alpha S_0}{R_\rho}\left[R_\rho(1-\phi_0)+1\right]. \tag{12}$$

It is noted that when $\phi_0 \ll 1$, $\Lambda \approx \alpha S_0$, whereas for $\phi_0 \lessapprox 1$ or $\alpha S_0 \ll 1$, $\Lambda \approx \phi_0(G-1)$. Eq. (12) exposes that smaller values of R_ρ imply higher values of the Λ, and thus higher values of the reduced gravity $g' = g\Lambda$. When $R_\rho < 1$ the suspension is initially stable from a bulk density perspective, whereas $R_\rho > 1$ implies the onset of a Rayleigh Taylor instability. When $R_\rho < 1$, in spite of the apparent stability of the system, plumes form in the upper layer, with little mixing in the lower layer (Schulte et al., 2016), a result that we confirm with our numerical simulations, as shown below. The present problem has only one external length scale, given by the characteristic size of the settling particles, d. In Stokes regime, for spherical particles, $d = \sqrt{\frac{18 w_s F(\phi_0)\nu}{g(G-1)}}$, where it is assumed that $\alpha S_0 \ll 1$. Here, $F(\phi_0)$ is a hindrance function ($0 < F \leq 1$) that accounts for the effect of particle concentration in the settling process (Davis and Acrivos, 1985). A second length scale may be obtained from salt water density inversion responsible for the plume release, by analogy to the plume release mechanism from thermal boundary layers in Rayleigh-Bénard convection. In this mechanism, at the onset of plume eruption there is a mass boundary layer whose thickness is given by a critical Rayleigh number: $Ra_c^{\mathrm{bl}} = \frac{g\Lambda_0\delta^3}{\nu D}$,

where the critical parameter Ra_c^{bl} has been measured between 100 and 1000 in thermal convection (Castaing et al., 1989; Zocchi et al., 1990), where Λ_0 is the relevant density difference that is commonly expressed in terms of a thermal or mass expansion coefficient. In the present case, $\Lambda_0 \equiv \Lambda(S_0, \phi_0 = 0) = \alpha S_0$. Assuming that Ra_c^{bl} is a constant that can be measured in this case (Ra_0), a second, Bénard-like length scale δ is obtained. Scaling by the particle length scale, we write

$$\frac{\delta}{d} = \theta (Sc\Lambda_0)^{-1/3} (G-1)^{1/2} R_w^{-1/2}, \tag{13}$$

with $\theta = \frac{Ra_0^{1/3}}{\sqrt{18}} \sim 1$ and

$$R_w = \frac{w_s F(\phi_0)}{(g\nu)^{1/3}}. \tag{14}$$

The velocity ratio R_w is independent on the salt concentration, but is implicitly dependent on the gravity. As in Stokes flow $w_s \propto g$, $R_w \propto g^{2/3}$, implying that R_w is actually a version of a particle buoyancy-viscous dissipation ratio. The problem can be thus defined in dimensionless terms by G, Sc, Λ (or Λ_0), R_ρ and R_w. Both Λ and R_ρ are implicit functions of ϕ_0 and αS_0.

From the definition of the length scale δ and the particle front velocity, $w_s F(\phi)$, a time scale is written as $\tau = \delta / w_s F$. In terms of the present choice of dimensionless variables,

$$\tau = \frac{1}{R_w} \left(\frac{D Ra_0}{\Lambda_0 g^2} \right)^{1/3}. \tag{15}$$

4 Numerical Simulations

The model equations described in section 2 are implemented in the solver *twoPhaseEulerFoam* of the open source software *OpenFOAM*. The domain is two dimensional with periodic boundary conditions in the horizontal direction, solid wall in the bottom and stress free at the top. The dimensionless parameter R_ρ has been set between 0.058 and 2.88, while R_w is between 2.4×10^{-6} and 0.46. For all the simulations, $G - 1 = 1.7$, $Sc = 700$ and $\Lambda_0 = 0.0245$.

5 Results and discussion

The present numerical simulations show that the excess density parameter R_ρ marks a transition from a Rayleigh-Taylor mode of mixing, including the upper and lower layers and a convective mode featuring the release of plumes and subsequent mixing in the upper layer. An example of the Rayeigh-Taylor mechanism, corresponding to $R_\rho > 1$ is shown in Figures 1 for the salt concentration field. A characteristic of the Rayleigh-Taylor mode of convection is the symmetry of the mixing layer with the middle plane. A summary of the two observed flow regimes in the present set of simulations is depicted in Figure 4.

The salt and particle transfer process is significantly different when $R_\rho < 1$. This is exemplified in Figure 2, for $R_\rho = 0.29$ and $R_w = 0.36$. In both cases, the excess density of the upper layer has been kept constant. Although mixing does occur, it is confined to the plane above the sediment layer, located at a distance equal $w_s t$ below the horizontal centerline. The effect of particle diffusivity is slight and, in the present set of numerical simulations it has been found that particle diffusion became irrelevant shortly after the

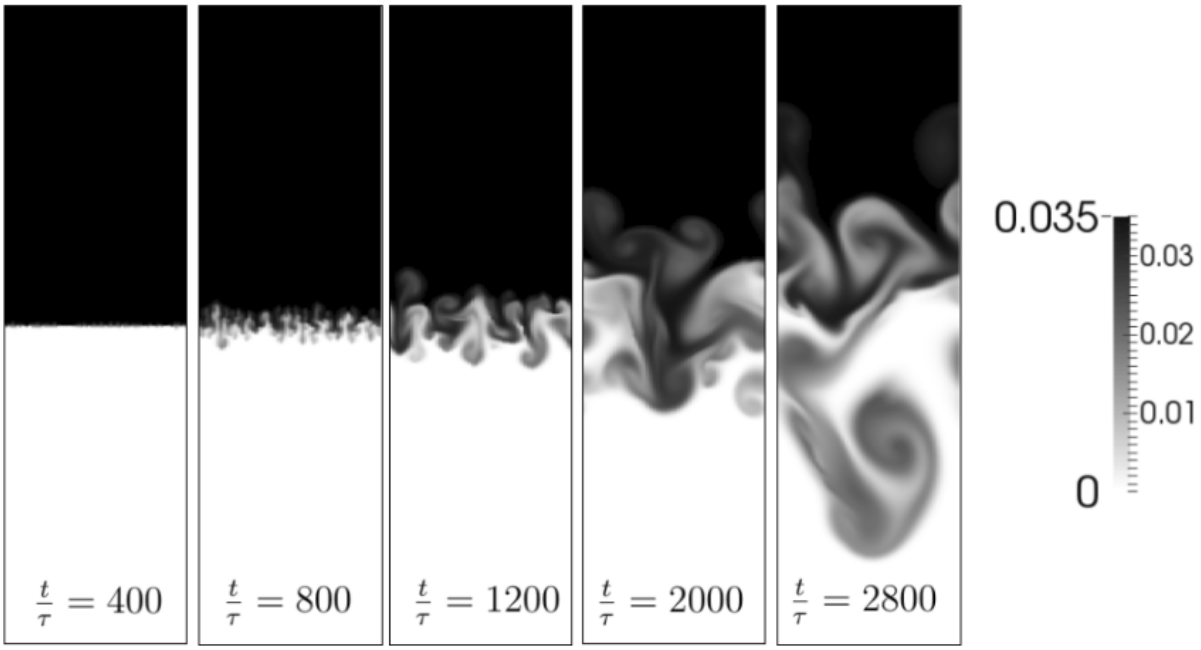

Figure 1: Salt concentration for simulation with $R_\rho = 2.88$ and $R_w = 0.46$. In this case, the particle concentration field is very similar to the salt conentration at the specified values of time.

onset of mixing. However, although there is not enough potential energy in the system to cause a complete overturning of the particle layer, there may be a significant particle interface erosion due to vorticity near the interface. This is depicted on Figure 3, where for dimensionless times in excess of about 1000 the particle interface is no longer horizontal and some resuspension to the upper layer occurs. This process resembles the mixing of strongly stratified density interfaces in front of grid-induced turbulence (Fernando, 1991). An additional comparison between both flow modes is depicted on the horizontal rms of the salt concentration fluctuations in Figures 6 and 7 for $R_\rho > 1$ and $R_\rho < 1$, respectively. A large difference in the penetration depth of the salt layer into the bottom half can be observed. In the case with $R_\rho < 1$, the interface of salt fluctuations closely follows the interface of the sedimenting particles at $w_s t$.

Figure 5 shows the dimensionless critical time in terms of the dimensionless parameter δ/d (Eq. 13). Admittedly, the dynamics is not purely explained by the Bénard instability mechanism as in all the cases the plumes depart above the initial density inversion layer of time-dependent thickness $w_s t$. However, a comparison between the dimensionless critical time and δ/d shows a clear correlation, which gives a strong suggestion of this mechanism being dominant in the onset of mixing.

When $R_\rho < 1$, the dimensionless parameter R_w controls the mixing in the upper layer. At constant particle concentration, the mean vertical flow velocity at any particular vertical coordinate can be written as $\bar{u} = \phi_0 \bar{u}_s + (1-\phi_0)\bar{u}_l$, where $\bar{u}_s$ and $\bar{u}_l$ are the absolute velocities of the solid and liquid phases, respectively. Noting that the settling velocity, corresponding to the relative velocity between the solid and liquid phase can be related to u_s as $\bar{u}_s = w_s + \bar{u}_l$ and that in the present system there is no vertical mean flow ($\bar{u} = 0$), then $\bar{u}_l/(g\nu)^{1/3} = -\phi_0 R_w$. This implies that at equal concentration and fluid viscosity, the higher the value of R_w, the higher the upwards flow of fresh (light) water into the salt (heavy) water layer. An example of this effect is shown in Figure 8. An additional

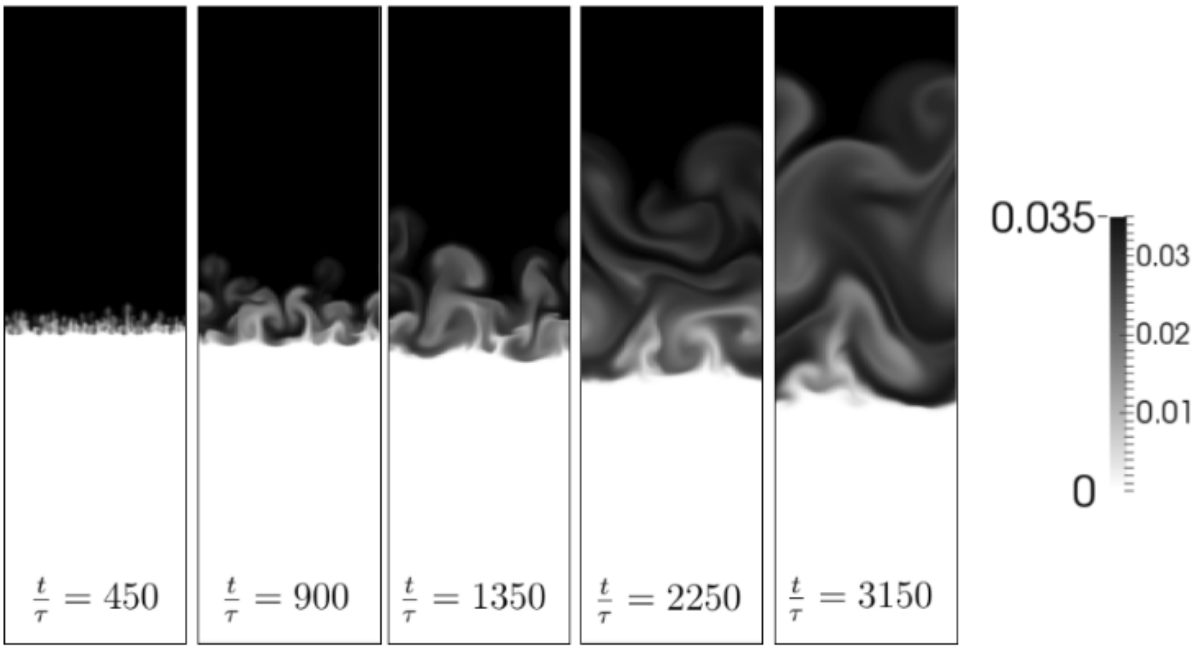

Figure 2: Salt concentration for simulation with $R_\rho = 0.29$ and $R_w = 0.36$.

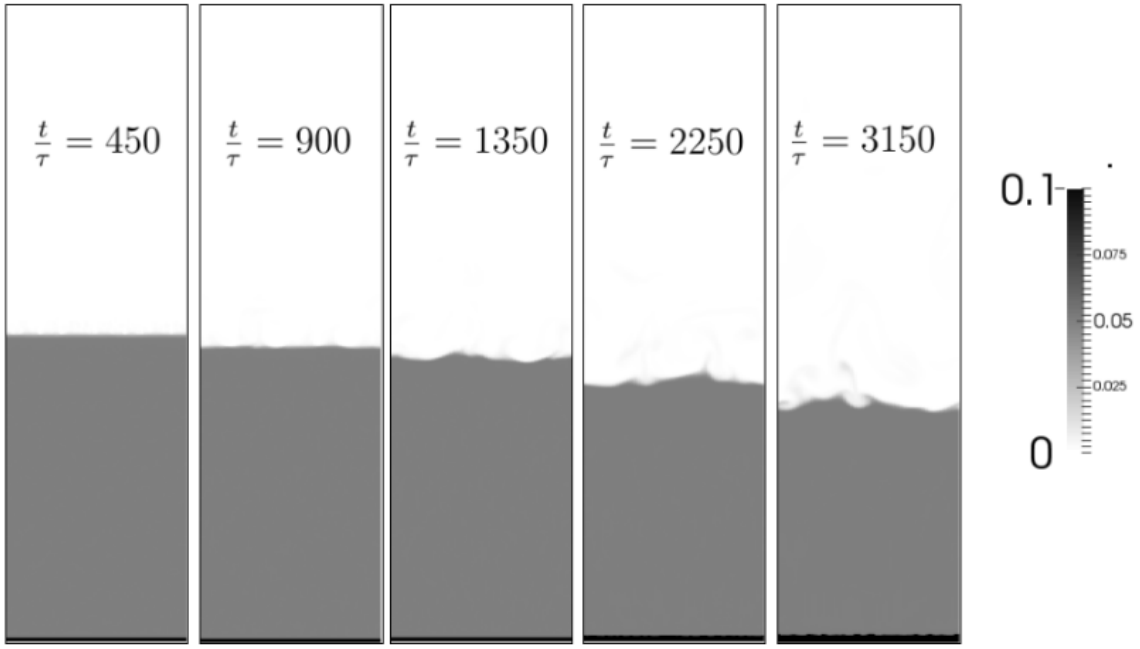

Figure 3: Particle concentration for simulation with $R_\rho = 0.29$ and $R_w = 0.36$.

consequence of high values of R_w is that in the computational domain particles smother the bottom of the reservoir faster. From a mass balance, it is obtained that in the absence of mixing in the bottom layer, the sediment height growth rate is $\dot{h}_s \approx \frac{w_s \phi_0}{\phi_m - \phi_0}$, with ϕ_m the value of the loose packing concentration at the bottom.

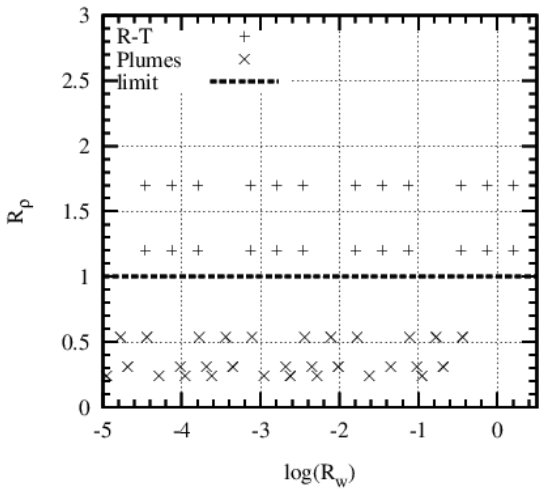

Figure 4: Summary of simulations in the space of parameters (R_ρ, R_w). Symbols indicate whether the mixing is controlled by the Rayleigh-Taylor instability or by plumes.

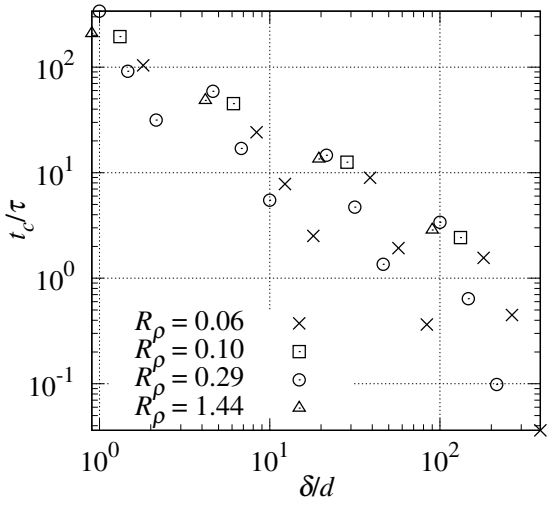

Figure 5: Dimensionless critical time in terms of the dimensionless parameter δ/d

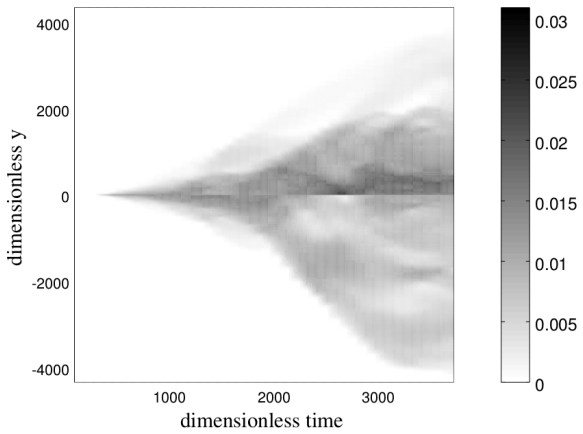

Figure 6: rms fluctuations of salt concentration as a function of the vertical coordinate and the dimensionless time for the case $R_\rho = 2.88$ and $R_w = 1.46$ (Rayleigh-Taylor).

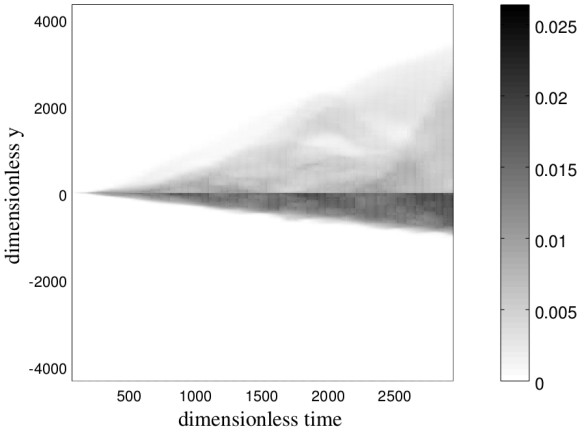

Figure 7: rms fluctuations of salt concentration as a function of the vertical coordinate and the dimensionless time for the case $R_\rho = 0.29$ and $R_w = 9.8 \times 10^{-1}$.

6 Conclusions

The present numerical simulations reveal that the excess density parameter, R_ρ, explains the transition from a Rayleigh-Taylor flow to a plume detachment regime in the upper layer. In the present set of non-dilute runs the existence of strong stratification induced by non-dilute particle concentrations gives way to a comparatively weaker, albeit non-diffusive, mixing process. The present simulations suggest that the onset of mixing is strongly dependent of the thickness of the (unstable) mixing layer induced by the particle layer settling relative to the characteristic size of sediments. It is left to interpret from high resolution numerical simulations and experiments the intriguing and certainly more

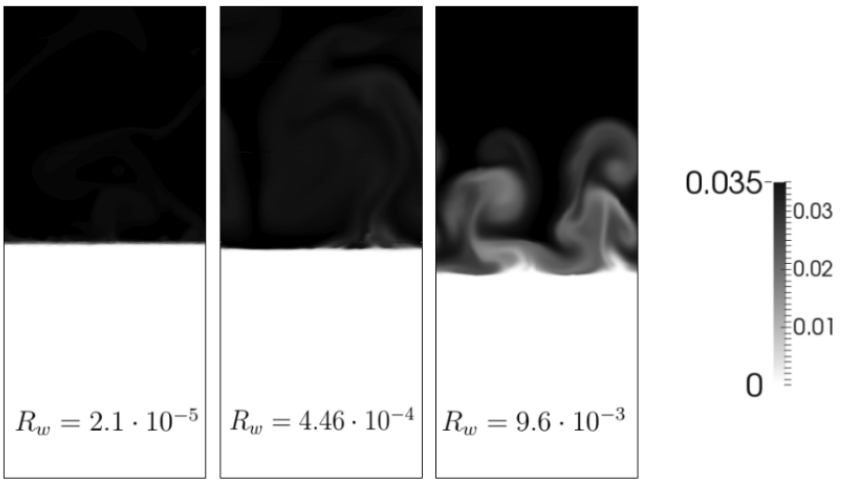

Figure 8: Snapshots of Salt concentration for simulation in $t/\tau = 2500$ for three R_w with $R_\rho = 0.1$.

complex nature of the subsequent mixing processes.

References

Castaing, B., Gunaratne, G., Heslot, F., Kadanoff, L., Libchaber, A., Thomae, S., Wu, X.-Z., Zaleski, S., and Zanetti, G. (1989). Scaling of hard thermal turbulence in Rayleigh-Bénard convection. *J. Fluid Mech.*, 204:1–30.

Davis, R. H. and Acrivos, A. (1985). Sedimentation of noncolloidal particles at low Reynolds numbers. *Annu. Rev. Fluid Mech.*, 17(1):91–118.

Enwald, H., Peirano, E., and Almstedt, A.-E. (1996). Eulerian two-phase flow theory applied to fluidization. *Int. J. Multiphase Flow*, 22:21–66.

Fernando, H. (1991). Turbulent mixing in stratified fluids. *Annu. Rev. Fluid Mech.*, 23(1):455–493.

Gidaspow, D. (1986). Hydrodynamics of fiuidizatlon and heat transfer: Supercomputer modeling. *Appl. Mech. Rev.*, 39(1):1–23.

Mulder, T., Syvitski, J. P. M., Migeon, S., Faugères, J.-C., and Savoye, B. (2003). Marine hyperpycnal flows: initiation, behavior and related deposits. A review. *Mar. Pet. Geol.*, 20(6-8):861–882.

Schiller, L. and Naumann, Z. (1935). A drag coefficient correlation. *Vdi Zeitung*, 77(318):51.

Schulte, B., Konopliv, N., and Meiburg, E. (2016). Clear salt water above sediment-laden fresh water: interfacial instabilities. *Phys. Rev. Fluids*, 1:012301.

Zocchi, G., Moses, E., and Libchaber, A. (1990). Coherent structures in turbulent convection, an experimental study. *Phys. A Stat. Theor. Phys.*, 166(3):387–407.